Next Research 2 (2025) 100439

Contents lists available at ScienceDirect

Next Research

journal homepage: www.elsevier.com/locate/nexres

Bioremediation of soil contaminated with cassava mill effluents - A structural, functional, and metagenomics approach

A.T. Ajao[a,*], S. Awe[a], W.T. Aborisade[a], F.A. Jimoh[a], F.J. Ajao[b]

[a] Department of Microbiology, Faculty of Pure and Applied Sciences, Kwara State University, Malete, Nigeria
[b] Department of Computer Science, Faculty of Information and Communication Technology, Kwara State University, Malete, Nigeria

ARTICLE INFO

Keywords:
Cassava mill effluent (CME)
Bioremediation
Cyanide-degrading bacteria
Molecular docking
Soil restoration
Heavy metal reduction

ABSTRACT

Cassava mill effluent (CME) is a toxic pollutant that acidifies soil, accumulates cyanide and heavy metals, and drastically reduces soil fertility and microbial diversity. To address this, we evaluated the bioremediation potential of selected cyanide-degrading bacteria (*Pseudomonas fluorescens, Bacillus pumilus, Pseudomonas putida*, and *Pseudomonas stutzeri*) in CME-polluted soil using an integrated approach combining enzymatic assays, metagenomic profiling, and molecular docking analyses. In laboratory microcosms, these strains significantly improved soil conditions over 20 days: soil pH increased from ~4.8 to ~7.4, cyanide levels fell by over 80 %, and key heavy metals (e.g., Cu^{2+}, Cd^{2+}) were eliminated or sharply reduced. Heterotrophic bacterial counts rebounded, and enzymatic activity (nitrilase, cyanide dihydratase) correlated with the degradation of cyanide. Metagenomic sequencing revealed a restored and more diverse microbial community dominated by beneficial genera such as *Pseudomonas* and *Bacillus* after treatment. Molecular docking simulations confirmed cyanide binding to the bacterial enzymes, supporting the degradation mechanism. Our findings demonstrate that a targeted microbial consortium can detoxify CME-contaminated soils and restore soil health. This integrative structural–functional strategy provides a promising framework for sustainable remediation of cassava processing waste in agricultural lands.

1. Introduction

Cassava (*Manihot esculenta* Crantz) is a staple crop of immense importance in tropical and subtropical regions, consumed by over two billion people globally and serving as the principal source of carbohydrates for >700 million individuals. In Nigeria, cassava plays a dual role as both a food security crop and a key driver of rural livelihoods and agro-industrial development. However, the widespread processing of cassava roots into products such as *garri, fufu*, and starch generates vast quantities of cassava mill effluent (CME)—a liquid waste often discharged indiscriminately into the environment without prior treatment. CME contains toxic components, including cyanogenic compounds, phenolic substances, and heavy metals, which contaminate soil and water bodies, alter essential physicochemical soil properties, disrupt microbial ecosystems, and contribute to long-term ecological degradation.

Numerous studies have documented the harmful effects of CME, including soil acidification, increased electrical conductivity, cyanide accumulation, reduced microbial diversity, and diminished agricultural productivity. These impacts are especially pronounced in Nigerian states such as Kwara, Ogun, Benue, and Imo, where cassava processing is intensive. In areas like Ilorin, farmlands adjacent to cassava mills have become severely degraded, characterized by declining soil fertility, loss of microbial biomass, and contamination of groundwater sources. Despite the severity of these challenges, current remediation efforts remain largely ineffective, relying on unsustainable physical and chemical methods that are both cost-prohibitive and ecologically intrusive.

While prior studies have characterized the composition of cassava mill effluent and its environmental impacts, limited research has explored bioremediation strategies for restoring polluted soils [1].

Abbreviations: CME, (Cassava Mill Effluent); CFU/g, (Colony-Forming Units per Gram); CMM, (Cyanide Mineral Medium); EC, (Electrical Conductivity); OM, (Organic Matter); CEC, (Cation Exchange Capacity); WHC, (Water Holding Capacity); FDA, (Fluorescein Diacetate); NaOH, (Sodium Hydroxide); HCl, (Hydrochloric Acid); OD600, (Optical Density at 600nm); PCR, (Polymerase Chain Reaction); DNA, (Deoxyribonucleic Acid); BLASTn, (Basic Local Alignment Search Tool – nucleotide); AAS, (Atomic Absorption Spectrophotometry); PEG, (Polyethylene Glycol); ANOVA, (Analysis of Variance); SPSS, (Statistical Package for the Social Sciences); PDB, (Protein Data Bank); CynD, (Cyanide Dihydratase); CynS, (Cyanide Synthase); MR, (Methyl Red); VP, (Voges–Proskauer); OTU, (Operational Taxonomic Unit); MEGA X, (Molecular Evolutionary Genetics Analysis X); QIIME, (Quantitative Insights Into Microbial Ecology).

* Corresponding author.
E-mail address: abdullahi.ajao@kwasu.edu.ng (A.T. Ajao).

https://doi.org/10.1016/j.nexres.2025.100439
Received 26 February 2025; Received in revised form 17 May 2025; Accepted 20 May 2025
3050-4759/© 2025 Elsevier Ltd. All rights are reserved, including those for text and data mining, AI training, and similar technologies.

In particular, the role of microbial communities—especially cyanide-degrading bacteria—in detoxifying CME remains poorly understood [2]. The bioremediation potential of indigenous microorganisms also remains underexplored, despite their inherent adaptability to local environmental conditions. There is a pressing need to develop and validate biological approaches that are environmentally sustainable, cost-effective, and scalable.

Bioremediation, particularly through the use of indigenous cyanide-degrading bacteria, presents a natural and effective solution for restoring soil health, detoxifying pollutants, and regenerating microbial diversity. This technique harnesses the metabolic capabilities of microorganisms, such as bacteria and fungi, to degrade or transform toxic compounds into less harmful forms, ultimately restoring soil structure and function [3]. By leveraging the metabolic versatility of microbial communities in polluted environments, bioremediation offers a low-cost, eco-friendly method for reversing CME-induced degradation [4]. Tailoring bioremediation interventions to site-specific conditions enhances their effectiveness and scalability, promoting the reduction of toxic loads, restoration of microbial equilibrium, and improvement in key soil quality indicators. Beyond pollution control, adopting bioremediation supports sustainable agriculture, environmental rehabilitation, and public health protection in affected communities.

Critically, effective bioremediation depends not only on identifying functional microbial strains but also on understanding the structural and biochemical mechanisms underlying pollutant degradation. Assessing the enzymatic activity of key detoxifying enzymes such as nitrilase and cyanide dihydratase, along with evaluating their substrate specificities via molecular docking, can provide valuable insights into the efficiency of cyanide biodegradation. Furthermore, metagenomic analysis is essential for monitoring shifts in microbial diversity, community succession, and overall ecosystem recovery post-intervention. However, the integrated application of these tools—enzyme assays, molecular modeling, and metagenomics—has rarely been used in tandem within CME-polluted contexts, particularly in the Nigerian setting. Addressing this knowledge gap, the present study adopts a novel, multidisciplinary framework—the first of its kind in Nigeria—to evaluate the bioremediation potential of selected indigenous cyanide-degrading bacteria. This study combines physicochemical soil characterization, microbial enumeration, quantitative enzyme activity assays, molecular docking simulations, and metagenomic profiling to assess both the functional performance and ecological outcomes of bioremediation. By integrating these multidisciplinary techniques, this research provides a comprehensive evaluation of the bioremediation capacity of indigenous cyanide-degrading bacteria in CME-contaminated soils. This holistic approach not only deepens understanding of microbial degradation mechanisms at biochemical and structural levels but also offers a robust framework for monitoring ecological restoration and soil health improvement in polluted environments. It enables a multidimensional assessment of bioremediation effectiveness—from enzyme-substrate interactions to microbial ecosystem recovery—offering novel insights into sustainable pollution management within agro-industrial systems. Addressing this knowledge gap, the present study adopts a novel, multidisciplinary framework—the first of its kind in Nigeria—to evaluate the bioremediation potential of selected indigenous cyanide-degrading bacteria. This research combines physicochemical soil characterization, microbial enumeration, quantitative enzyme activity assays, molecular docking simulations, and metagenomic profiling to comprehensively assess the functional performance and ecological outcomes of bioremediation. Through this integrated approach, the study aims to characterize cassava mill effluent-contaminated soils, isolate and identify effective microbial strains, evaluate the enzymatic efficiency and pollutant interactions of these isolates, monitor the restoration of microbial diversity, and assess progressive improvements in soil quality over time. By bridging structural, biochemical, and ecological perspectives, this holistic strategy not only advances our understanding of microbial degradation mechanisms but also establishes a robust framework for the practical implementation of sustainable pollution control and ecological restoration in agro-industrial ecosystems.

2. Materials and methods

2.1. Study area and sampling site description

The study was conducted in Ilorin, the capital city of Kwara State, Nigeria, located at approximately 8.4900° N latitude and 4.5500° E longitude. Ilorin hosts numerous cassava mills that process cassava into garri, fufu, and starch, generating large volumes of cassava mill effluent (CME). For this study, soil samples were collected from eight identified cassava processing zones (S1–S8) across Ilorin Metropolis (Fig. 1), based on proximity to effluent discharge points.

3. S1-S8: selected cassava processing sites

3.1. Soil Sampling and physicochemical characterization

Soil samples were collected from a cassava processing site contaminated with effluent, within a 500-meter radius of the discharge point, at depths of 0–15 cm, 15–30 cm, and 30–45 cm. Samples were stored in sterile containers and transported to the laboratory for analysis.

Physicochemical parameters were determined using standard protocols. Soil pH and electrical conductivity (EC) were measured in a 1:2 soil–water suspension using a Thermo Scientific Orion 5-Star pH meter and YSI ProPlus conductivity meter (ASTM D4972; D1125). Organic matter (OM) content was estimated via the Loss-on-Ignition method (ASTM D2974), while cation exchange capacity (CEC) was measured using the ammonium acetate method. Total nitrogen (N) and phosphorus (P) were quantified using the Kjeldahl and molybdenum blue methods, respectively, with absorbance read on a Shimadzu UV-2600 spectrophotometer. Heavy metals including Fe^{2+}, Mn^{2+}, Cu^{2+}, Zn^{2+}, Cr^{6}, Pb^{2+}, Ni^{2+}, and Cd^{2+} were analyzed using a PerkinElmer AAnalyst 400 atomic absorption spectrophotometer. Particle size distribution was assessed using either the hydrometer method (ASTM D422) or laser diffraction (Malvern Mastersizer 3000), while water holding capacity (WHC) was evaluated following ASTM D4647.

3.2. Enumeration of heterotrophic bacteria

Ten-fold serial dilutions of contaminated soil samples were prepared. Aliquots (1 mL) from appropriate dilutions (10^{-3} to 10^{-9}) were plated on nutrient agar using the pour plate method and incubated at 37 °C for 24 h [5]. Colonies were counted and results expressed as colony-forming units per gram of soil (CFU/g).

3.3. Biochemical and molecular characterization of the isolates

Pure colonies were obtained through successive subculturing and characterized using standard morphological and biochemical tests, including catalase, oxidase, urease, indole, methyl red (MR), Voges–Proskauer (VP), citrate, coagulase, and sugar fermentation assays (Bhutia et al., 2022). Genomic DNA was extracted using the ZymoBIOMICS™ DNA Miniprep Kit (Zymo Research, USA), optimized for Gram-positive and Gram-negative bacteria. Bacterial pellets were lysed by bead beating, and DNA was purified via spin columns. DNA was eluted in nuclease-free water and quantified using a NanoDrop ND-1000 spectrophotometer. The 16S rRNA gene was amplified using primers 27F and 1492R [6] in a 50 μL PCR mix containing GoTaq Green Master Mix. PCR conditions included initial denaturation at 94 °C (5 min), 35 cycles (94 °C for 1 min, 55 °C for 1 min, 72 °C for 1.5 min), and a final extension at 72 °C for 7 min. Amplicons were visualized on 1 % agarose gels, purified using PEG-NaCl, and sequenced via Sanger sequencing [7]. Edited sequences were aligned in BioEdit v7.2.5 and

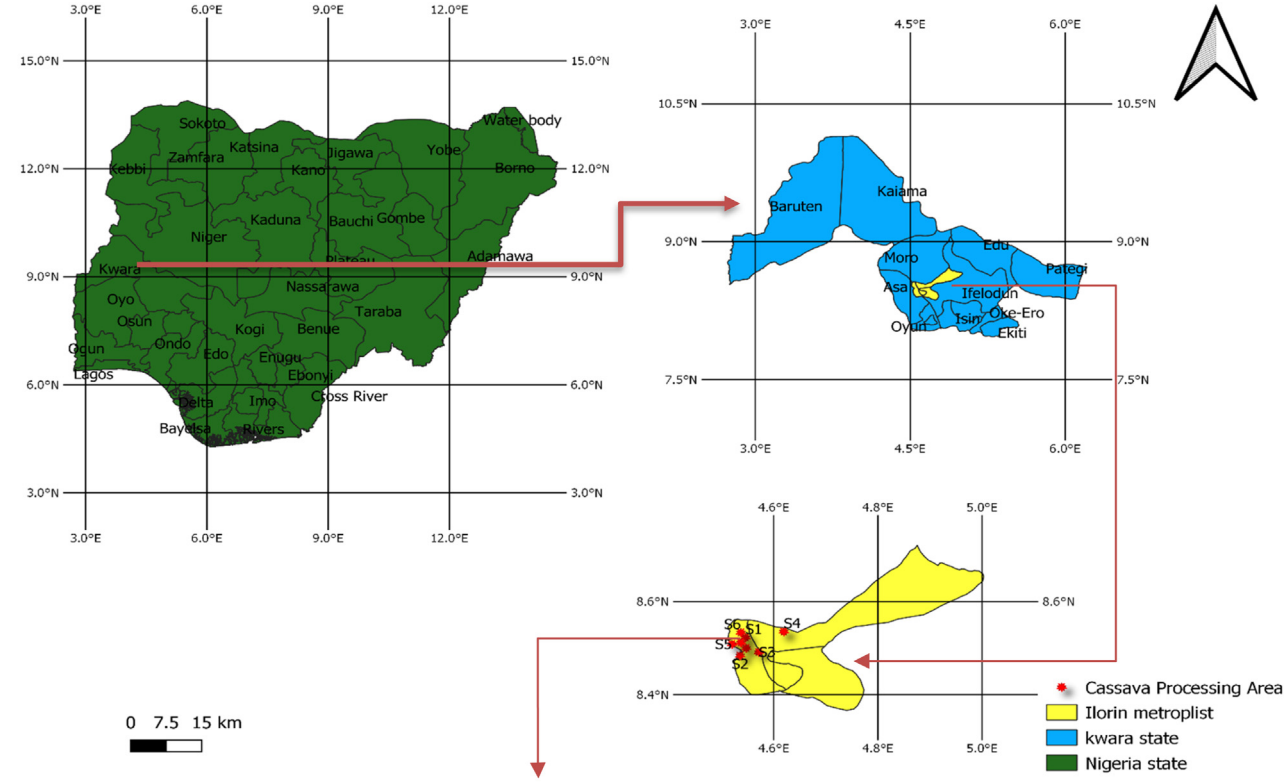




Fig. 1. Map of the Cassava Processing Areas in Ilorin Metropolis.

identified using BLASTn (NCBI GenBank). Sequences with ≥97 % similarity were assigned species-level identity. A Neighbor-Joining phylogenetic tree was constructed in MEGA X with 1000 bootstrap replicates using ClustalW-aligned sequences.

3.4. Soil enzyme activity assays

To assess microbial functional activity, soil enzyme assays were conducted on control and CME-contaminated microcosms. Dehydrogenase activity was determined by fluorescein diacetate (FDA) hydrolysis. One gram of soil was incubated with 1 mL of 1 % FDA in 100 mM Tris–HCl buffer (pH 8.0) at 30 °C for 30 min. The reaction was stopped by adding 0.5 M $CaCl_2$, centrifuged at 10,000 × *g* for 5 min, and fluorescence measured at 490/514 nm [8]. Catalase (EC 1.11.1.6) and urease (EC 3.5.1.5) activities were measured following Afangide *et al.* (2021), with results expressed in units per gram of soil. All tests were performed in triplicate.

3.5. Bioremediation microcosm setup and soil treatment

Microcosms were established in sterile containers (11″ × 8″ × 2″) containing 1 kg of CME-contaminated or control soil. Soil pH was adjusted to 6.5–7.5 using sterile 0.1 M NaOH or HCl, and molasses was

added (5–10 % v/w) as a carbon source. Moisture was maintained at 20 % using sterile distilled water, and aeration was done weekly. Cyanide-degrading isolates (IBR-001 to IBR-004) were cultured in Tryptic Soy Broth at 30 °C for 18–24 h, centrifuged (4000 rpm), washed in 0.87 % NaCl, and resuspended to OD_{6nn} = 0.6–1.0. A 5 % (v/v) suspension was added per microcosm and incubated at 30 ± 3 °C for 20 days.

3.6. Enzyme activity assays of cyanide-degrading bacterial isolates

Crude enzyme extracts of isolates (IBR-001 to IBR-004) were prepared by sonication in 100 mM Tris–HCl (pH 8.0), followed by centrifugation. Each 1 mL reaction contained 100 µL of enzyme extract, 100 µL of substrate (10 mM KCN, l-cysteine, thiosulfate+KCN, or benzyl cyanide for CynD, CynS, rhodanese, and nitrilase respectively), and 800 µL of buffer. Absorbance was measured at 600 nm (CynD, CynS), 412 nm (rhodanese), and 405 nm (nitrilase). Enzyme activity (U/mL) was calculated using:

$$\text{Enzyme Activity (U/mL)} = \frac{\Delta A \times V_t}{\varepsilon \times l \times V_e \times t}$$

Where:

- ΔA = change in absorbance (sample – blank)
- V_t = total volume (mL)
- ε = molar extinction coefficient ($mM^{-1}cm^{-1}$)
- l = path length (cm)
- V_e = volume of enzyme used (mL)
- t = incubation time (min)

Values were expressed as mean ± SD.

3.7. Metagenomic DNA extraction and bioinformatics analysis

Soil DNA was extracted using the ZymoBIOMICS DNA Miniprep Kit, and the V3–V4 region of the 16S rRNA gene was amplified and sequenced using the Illumina MiSeq platform. Sequence data were processed using QIIME, with diversity metrics (alpha and beta) computed to assess microbial richness and community structure.

3.8. Molecular docking configuration

Docking studies were conducted with AutoDock Vina to model cyanide binding to bacterial enzymes. Crystal structures of nitrilase (PDB: 6ZBY) and cyanide dihydratase (PDB: 8P41) were retrieved from the Protein Data Bank. Receptor structures were prepared using AutoDock Tools by removing water molecules, adding polar hydrogens, and assigning Gasteiger charges. The ligand (cyanide ion) and receptor were converted to PDBQT format. Docking was performed using a grid box centered at $x = 138.914505$, $y = 145.385207$, $z = 128.248698$, with dimensions of 40 × 40 × 40 Å and exhaustiveness set to 8. Docking results were saved in output.pdbqt and visualized using Discovery Studio Visualizer to analyze interactions such as hydrogen bonding, van der Waals forces, and binding energy.

3.9. Statistical analysis

All experimental data were subjected to statistical analysis using one-way Analysis of Variance (ANOVA) to evaluate significant differences among treatment groups. Where significant effects were observed, Tukey's Honest Significant Difference (HSD) post hoc test was applied to determine pairwise comparisons between group means. The level of significance (α) was set at $p < 0.05$ for all tests. Each treatment group included three replicates ($n = 3$), unless otherwise stated. Data were expressed as mean ± standard deviation (SD). All statistical computations were performed using IBM SPSS Statistics version 26.0. Significance values and statistical groupings are clearly presented in the respective tables. Additionally, enzyme-substrate interactions and molecular docking analyses were carried out using BIOVIA Discovery Studio Visualizer, as indicated in the figure legends and relevant sections.

4. Results

Table 1 presents the analysis of soil parameters across various sampling sites (S1–S8), revealing statistically significant differences ($p < 0.05$) in physicochemical and heavy metal profiles between cassava mill effluent (CME)-polluted soils and the control. Soil pH was markedly lower in all polluted sites (4.30–5.62) compared to the control (6.78), indicating acidification as a result of effluent contamination. Electrical conductivity (EC) was significantly higher in S1 (985 µS/cm) than in other sites, with the control showing the lowest value (155 µS/cm), reflecting elevated ionic concentrations in contaminated soils ($\boldsymbol{p} < 0.05$). Total nitrogen (17.10–22.12 mg/kg) and organic carbon (1.80–2.71 %) levels were significantly elevated in polluted sites relative to the control, suggesting nutrient enrichment, albeit still below optimal thresholds for soil health. Conversely, phosphorus levels were significantly lower in polluted soils (37.80–51.21 mg/kg) compared to the control (66.55 mg/kg), indicating disrupted nutrient dynamics and potential nutrient immobilization ($\boldsymbol{p} < 0.05$).

Cyanide concentrations were significantly elevated in polluted soils (S1–S7), (35.65–45.55 mg/kg) compared to the control (S8) (2.50 mg/kg), confirming cassava mill effluent as a major cyanide source. Heavy metals such as Fe, Zn, Cu, Ni, and Mn were also significantly higher in polluted soils, with Fe ranging from 18.33 to 32.45 mg/kg ($\boldsymbol{p} < 0.05$). However, levels of Pb and Cr^{6+} did not vary significantly across sites ($\boldsymbol{p} > 0.05$), suggesting their minimal contribution from cassava effluent. Bulk density and organic matter content were significantly greater in polluted sites than in the control ($\boldsymbol{p} < 0.05$), indicating increased soil compaction and organic accumulation due to effluent discharge. CME significantly alters soil properties, increasing cyanide and heavy metal concentrations, reducing soil quality, and impacting microbial health Table 2 shows the total heterotrophic bacterial (THB) and cyanide-degrading bacterial (CDB) counts in CME-contaminated soils and the control site (S8). THB counts were significantly lower in polluted sites (S1–S7) compared to the control, with the control site (S8) showing the highest THB count (8.93 log cfu/g). CDB counts were also significantly lower in the polluted sites, ranging from 3.36 to 4.49 log cfu/g, with S1 having the highest count. In contrast, the control site had the lowest CDB count (2.11 log cfu/g), likely due to the absence of cyanide, which stimulates the growth of cyanide-degrading bacteria in polluted soils. These results suggest that CME contamination reduces overall bacterial populations, including those capable of degrading cyanide. ANOVA and Tukey's post hoc tests confirmed significant differences ($\boldsymbol{p} < 0.05$) between control and polluted soils, indicating the suppressive effect of CME on microbial populations. The phenotypic identification of the cyanide-degrading bacterial isolates—IBR-001 (*Pseudomonas fluorescens*), IBR-002 (*Bacillus pumilus*), IBR-003 (*Pseudomonas putida*), and IBR-004 (*Pseudomonas stutzeri*)—was performed using Gram staining, cell morphology, spore formation, and standard biochemical tests, as detailed in **Table S1 (Supplementary Materials)**.

The enzymatic activity data identify the most promising bacterial isolates for further molecular investigations. Pseudomonas fluorescens demonstrated the highest activities for Cyanide Dioxygenase (0.37 U/mg) and Nitrilase (3.22 U/mg), positioning it as a strong candidate for cyanide detoxification studies. In contrast, Bacillus pumilus exhibited the highest Cyanide Dihydratase activity (3.33 U/mg), significantly exceeding that of all other isolates. Regarding Rhodanese activity, Pseudomonas stutzeri (0.35 U/mg) showed marginally higher activity than Pseudomonas fluorescens (0.30 U/mg). Based on these results, the two most potent enzyme producers—Cyanide Dihydratase from Bacillus pumilus and Nitrilase from Pseudomonas fluorescens—are considered optimal candidates for molecular docking studies with cyanide ions to elucidate their detoxification mechanisms (Table 3).

Table 1
Comparative analysis of physicochemical properties and heavy metal concentrations in cassava mill effluent-polluted soils and control site.

Soil Parameters (Units)	Sampling Sites/Value of Physicochemical Parameters							
	S1	S2	S3	S4	S5	S6	S7	S8
pH	4.30 ± 0.01^{a}	4.81 ± 0.01^{ab}	5.21 ± 0.01^{b}	5.32 ± 0.01^{b}	4.77 ± 0.01^{ab}	5.62 ± 0.01^{b}	4.89 ± 0.01^{ab}	6.78 ± 0.01^{c}
Electrical conductivity (μS/cm)	985 ± 7.07^{c}	755 ± 7.07^{ab}	882 ± 7.07^{b}	833 ± 7.07^{b}	825 ± 7.07^{b}	778 ± 7.07^{ab}	743 ± 7.07^{ab}	155 ± 7.07^{a}
Total nitrogen (mg/kg)	20.50 ± 0.01^{c}	17.10 ± 0.01^{ab}	18.40 ± 0.01^{ab}	22.12 ± 0.01^{c}	18.11 ± 0.01^{ab}	20.23 ± 0.01^{c}	21.77 ± 0.01^{c}	11.30 ± 0.01^{a}
Organic carbon (%)	2.60 ± 0.01^{c}	2.71 ± 0.01^{c}	1.80 ± 0.01^{ab}	2.25 ± 0.01^{ab}	2.53 ± 0.01^{c}	1.87 ± 0.01^{ab}	2.00 ± 0.01^{ab}	1.10 ± 0.01^{a}
Phosphorus (mg/kg)	44.03 ± 0.00^{ab}	51.21 ± 0.0^{ab}	44.45 ± 0.00^{ab}	37.80 ± 0.0^{a}	41.22 ± 0.00^{ab}	41.49 ± 0.00^{ab}	38.53 ± 0.00^{a}	66.55 ± 0.00^{c}
Particles (%)								
1.0 mm	7.91 ± 0.01^{a}	8.16 ± 0.01^{a}	7.73 ± 0.01^{a}	8.45 ± 0.01^{a}	7.35 ± 0.01^{a}	7.92 ± 0.01^{a}	8.0 ± 0.01^{a}	16.32 ± 0.01^{b}
1.4 mm	3.22 ± 0.01^{ab}	2.12 ± 0.01^{a}	3.56 ± 0.01^{ab}	2.33±0.01^{a}	3.00 ± 0.01^{ab}	2.47 ± 0.01^{a}	2.13 ± 0.01^{a}	7.86 ± 0.01^{c}
1.8 mm	3.26 ± 0.08^{ab}	2.32 ± 0.08^{a}	3.55 ± 0.08 ^{ab}	3.20 ± 0.08^{ab}	3.15 ± 0.08^{ab}	3.30 ± 0.08^{ab}	2.87 ± 0.08^{ab}	10.20 ± 0.08^{b}
3.0 mm	7.78 ± 0.01^{ab}	7.22 ± 0.01^{a}	8.28 ± 0.01^{ab}	7.27 ± 0.01^{a}	6.97 ± 0.01^{a}	8.10 ± 0.01^{ab}	7.52 ± 0.01^{a}	15.22 ± 0.01^{b}
Fine particles	35.11 ± 0.01^{ab}	38.55 ± 0.01^{b}	30.42 ± 0.01^{ab}	32.78 ± 0.01 ^{ab}	28.90 ± 0.01^{ab}	33.23 ± 0.01^{ab}	30.76 ± 0.01^{ab}	22.44 ± 0.01^{a}
Cyanide (mg/kg)	42.12 ± 0.01^{b}	45.55 ± 0.01^{b}	40.78 ± 0.01^{b}	38.87 ± 0.01^{b}	35.65 ± 0.01^{b}	38.67 ± 0.01^{b}	41.25 ± 0.01^{b}	2.50 ± 0.01^{a}
Bulk density (g/cm^{3})	1.52 ± 0.01^{b}	1.30 ± 0.01^{a}	1.37 ± 0.01^{b}	1.35 ± 0.01^{b}	1.40 ± 0.01^{b}	1.42 ± 0.01^{b}	1.52 ± 0.01^{b}	0.82 ± 0.01^{a}
Organic matter (%)	22.30 ± 0.00^{ab}	18.10 ± 0.00^{b}	16.10 ± 0.00^{b}	17.65 ± 0.00^{b}	20.35 ± 0.00^{ab}	21.45.± 0.00^{ab}	19.10 ± 0.00^{ab}	7.35 ± 0.00^{a}
Heavy Metals (mg/kg)								
Fe	32.45 ± 3.11^{c}	28.21 ± 1.20^{b}	18.45 ± 0.57^{a}	20.00 ± 2.15^{ab}	26.43 ± 3.00^{b}	23.70 ± 1.00^{ab}	21.10 ± 2.71^{ab}	18.33 ± 0.67^{a}
Mn^{+2}	5.66 ± 0.23^{b}	6.00 ± 0.41^{b}	6.11 ± 0.11^{b}	4.00 ± 0.01^{a}	5.23 ± 0.35^{ab}	6.23 ± 0.41^{b}	5.31 ± 0.71^{ab}	6.56 ± 1.56
Cu^{+2}	2.31 ± 0.01^{ab}	1.51 ± 0.01^{a}	1.67 ± 0.01^{a}	3.44 ± 0.01^{b}	3.37 ± 0.01^{b}	3.18 ± 0.01^{b}	3.30 ± 0.01^{b}	2.01 ± 0.01^{a}
Zn^{+2}	4.90 ± 0.00 ^{b}	4.10 ± 0.00 ^{b}	3.61 ± 0.00 ^{b}	3.40 ± 0.00^{b}	3.87.01 ± 0.0^{b}	3.55 ± 0.00^{b}	4.00 ± 0.00^{b}	3.48 ± 0.00^{a}
Cr^{6}	3.27 ± 0.03^{a}	4.11 ± 0.03^{b}	2.95 ± 0.03^{a}	3.15 ± 0.03^{a}	3.45 ± 0.03^{a}	3.20 ± 0.03^{a}	4.00 ± 0.03^{b}	ND
Pb^{+2}	2.10 ± 0.03^{b}	2.17 ± 0.03^{b}	2.25 ± 0.03^{b}	2.08 ± 0.03^{b}	2.72 ± 0.03^{b}	1.89 ± 0.03^{b}	2.11 ± 0.03^{b}	0.55 ± 0.02^{a}
Ni^{+2}	6.22 ± 0.03^{b}	5.71 ± 0.03^{b}	5.95 ± 0.03^{b}	6.00 ± 0.03^{b}	5.75 ± 0.03^{b}	6.20 ± 0.03 d	6.00 ± 0.03^{b}	1.55 ± 0.00^{a}

The data presented are expressed as the mean ± standard error (SE). A one-way ANOVA was conducted, and results with $p < 0.05$ indicate significant differences in means among groups. The control group is denoted as such. Different letters (a, b, c) signify significant differences in means among groups as determined by post-hoc tests, such as Tukey's HSD. **S8-CTRL**.

Table 2
Total heterotrophic and cyanide-degrading bacterial counts in soils contaminated with cassava mill effluent.

Sample	THB (log cfu/g)	CDB (log cfu/g)
S1	5.86 ± 0.59^{a}	4.49 ± 0.45^{ab}
S2	5.68 ± 0.57^{a}	3.36 ± 0.34^{b}
S3	5.51 ± 0.55^{a}	4.08 ± 0.40^{ab}
S4	5.81 ± 0.58^{a}	4.28 ± 0.43^{ab}
S5	6.62 ± 0.66^{a}	3.90 ± 0.39^{b}
S6	5.78 ± 0.58^{a}	4.40 ± 0.44^{ab}
S7	5.75 ± 0.58^{a}	3.43 ± 0.34^{b}
S8	8.93 ± 0.89^{a}	2.11 ± 0.21^{b}

The data presented are expressed as the mean ± standard error (SE). A one-way ANOVA was conducted, and results with $p < 0.05$ indicate significant differences in means among groups. The control group is denoted as such. All values have been log-transformed (log cfu/g). Different letters (a, b, c) signify significant differences in means among groups as determined by post-hoc tests, such as Tukey's HSD. S8: CTRL.

Fig. 2A illustrates the 20-day bioremediation process, showing a sharp decline in cyanide concentration alongside a steady rise in bacterial population. The increase in soil pH and concurrent reduction in total organic carbon (TOC) suggest enhanced microbial activity and progressive detoxification, confirming the effectiveness of the bioremediation strategy. Fig. 2B shows that during bioremediation, cation exchange capacity (CEC) and cyanide dioxygenase activity increased, indicating improved soil fertility and enzymatic degradation of cyanide. Dehydrogenase activity (DHA) also rose, reflecting active microbial metabolism, while electrical conductivity (EC) declined steadily, suggesting reduced ion concentration and pollutant load in the soil. Fig. 2C illustrates a progressive increase in urease (UA) and catalase (CA) activities over the 20-day bioremediation period, indicating enhanced enzymatic function and microbial activity. Simultaneously, soil pH rises steadily, while total organic carbon (TOC) declines sharply, reflecting improved soil quality and active organic matter degradation. These trends confirm effective bioremediation through biological processe. Table 4 reveals a progressive reduction in heavy metal concentrations in the soil over 20 days, demonstrating the effectiveness of the remediation process. Initial levels of Fe (32.45 ± 2.67 mg/g) decreased steadily to 8.10 ± 0.03 mg/g, while Mn^{2+} dropped from 5.66 ± 0.23 mg/g to 2.17 ± 0.03 mg/g. Copper (Cu^{2+}) was completely removed by Day 16, and cadmium (Cd^{2+}) became undetectable by Day 12, highlighting their rapid degradation. Zinc (Zn^{2+}) decreased from 4.30 ± 0.00 mg/g to 2.08 ± 0.03 mg/g, and chromium (Cr^{6}) showed a significant reduction from 3.27 ± 0.01 mg/g to 0.72 ± 0.03 mg/g. Lead (Pb^{2+}) and nickel (Ni^{2+}) also demonstrated substantial declines, reaching 0.89 ± 0.03 mg/g and 1.78 ± 0.03 mg/g, respectively, by Day 20. These reductions were markedly better compared to the control values, which showed minimal natural attenuation. The findings indicate a highly effective remediation process, particularly for Cu^{2+} and Cd^{2+}, which were removed completely, emphasizing the potential for efficient heavy metal bioremediation.

Fig. 3a illustrates the correlation among physicochemical properties, microbial activities, and cyanide concentration across different time points. The first principal component (PC1), which explains 76.0 % of the total variance, distinctly separates parameters such as cyanide, total organic carbon (TOC), and electrical conductivity (EC), which cluster on the right, from those associated with microbial and enzymatic activities on the left. Soil pH aligns negatively with PC1 and PC2, suggesting a distinct behavior compared to other variables. Variables like cyanide, TOC, and EC show strong positive correlations with each other and are negatively associated with microbial indicators such as urease (UA), dehydrogenase (DHA), catalase (CA), and bacterial count, indicating effective detoxification and microbial resurgence during the bioremediation process.

Fig. 3b displays the PCA biplot for heavy metals detected in the polluted soil. PC1 explains 81.3 % of the total variance, while PC2 accounts for 15.0 %. Most of the metals—Zn, Pb, Mn, Cr, Ni, and Fe—are closely aligned, indicating a strong positive correlation and a likely common source or behavior in the contaminated environment. Cadmium (Cd), however, separates from the cluster along PC2, indicating a distinct distribution or response compared to the other metals. The spatial distribution of the numbered points (sampling days or sites) also reflects temporal or spatial variations in metal concentration trends during the bioremediation process. Together, these PCA analyses reveal clear clustering and directionality among the parameters, supporting the effective-

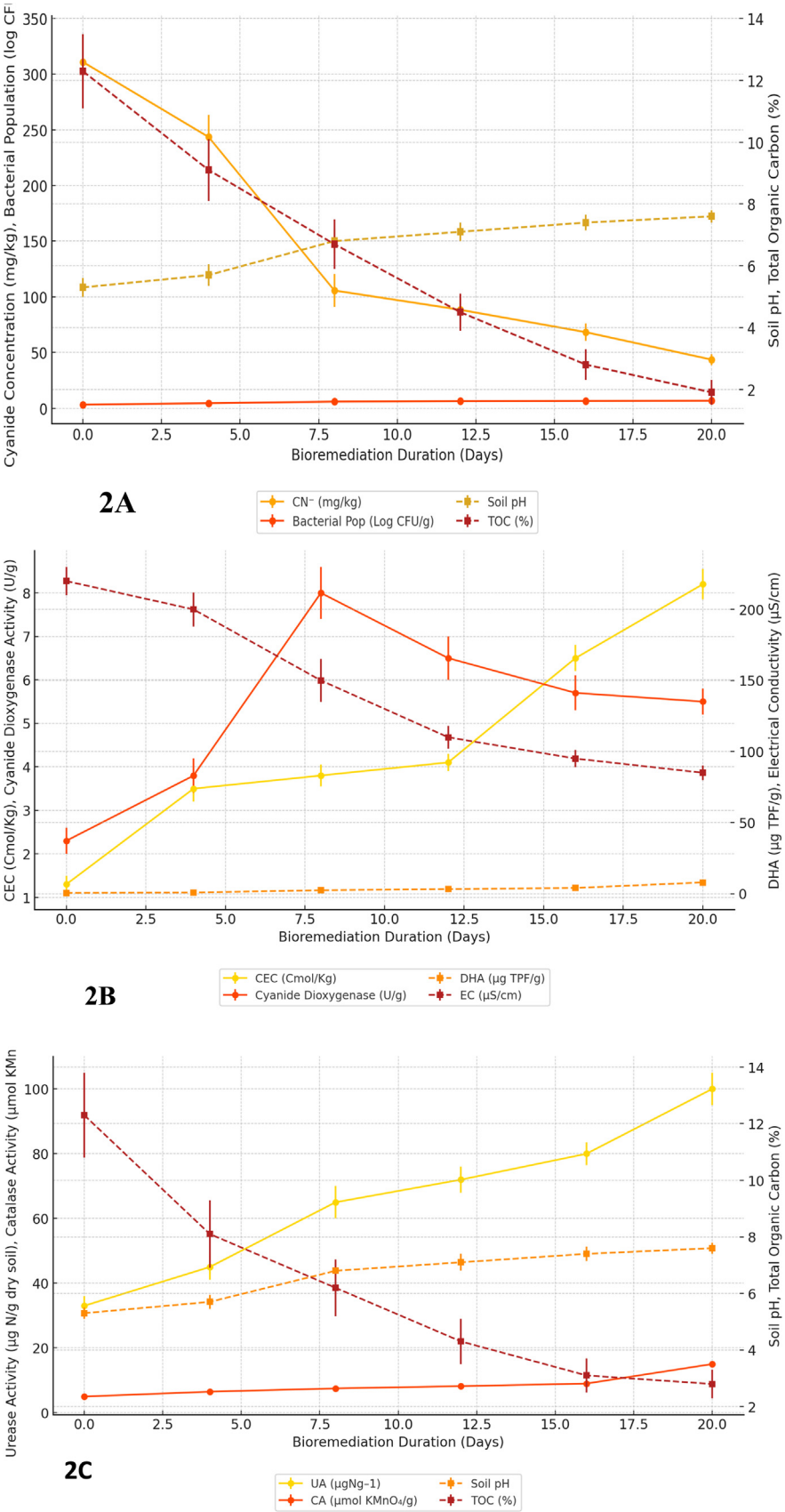


Fig. 2. Temporal variation of key bioremediation indicators across 20 days. The graphs illustrate: (A) Cyanide concentration and bacterial population versus soil pH and TOC; (B) CEC and cyanide dioxygenase activity versus DHA and EC; and (C) Urease and catalase activity versus soil pH and TOC. Error bars represent standard deviation across replicate measurements.

Table 3
Specific enzyme activities (u/mg protein) of bacterial isolates involved in cyanide degradation.

Isolates	Cyanide Dioxygenase	Cyanide Dihydratase	Nitrilase	Rhodanese
Pseudomonas fluorescens	0.37 ± 0.02[a]	0.45 ± 0.00[b]	3.22 ± 0.03[a]	0.30 ± 0.05[a]
Bacillus pumilus	0.20 ± 0.01[b]	3.33 ± 0.00[b]	0.23 ± 0.01[b]	0.15 ± 0.02[b]
Pseudomonas putida	0.30 ± 0.01[b]	0.01 ± 0.00[c]	0.28 ± 0.02[b]	0.16 ± 0.03[b]
Pseudomonas stutzeri	0.25 ± 0.03[b]	0.55 ± 0.02[b]	ND	0.35 ± 0.02[a]

The data presented are expressed as the mean ± standard error (SE). A one-way ANOVA was conducted, and results with $p < 0.05$ indicate significant differences in means among groups. The control group is denoted as such. Values that were not detected or are not applicable are indicated accordingly as ND. Different letters (a, b, c) signify significant differences in means among groups as determined by post-hoc tests, such as Tukey's HSD. ND:Not Detected.

Table 4
Temporal changes in heavy metal concentrations (mg/g) during soil bioremediation.

Days	Heavy Metals (mg/kg)							
	Fe^{+2}	Mn^{+2}	Cu^{+2}	Zn^{+2}	Cr^{6}	Pb^{+2}	Ni^{+2}	Cd^{+2}
0	32.45 ± 2.67[b]	5.66 ± 0.23[ab]	2.36 ± 0.01[a]	4.30 ± 0.00 [ab]	3.27 ± 0.01[a]	2.72 ± 0.03[a]	6.22 ± 0.03[ab]	0.25 ± 0.031[a]
4	25.00 ± 0.23[b]	5.00 ± 0.41[ab]	1.11±0.11[a]	4.00 ± 0.01[ab]	3.03 ± 0.35[a]	2.33 ± 0.80[a]	5.31 ± 0.71	0.07 ± 0.00[a]
8	12.08 ± 0.01[b]	4.51 ± 0.01[ab]	0.67±0.01[ab]	3.44 ± 0.01[ab]	2.77 ± 0.01[a]	2.18± 0.01[a]	4.30 ± 0.01[ab]	0.01 ± 0.00[a]
12	9.30 ± 0.00 [c]	4.10 ± 0.00[b]	0.03 ± 0.00[a]	3.40 ± 0.00[b]	1.87 ± 0.0[a]	1.55 ± 0.00[a]	3.30 ± 0.00[b]	ND
16	8.27 ± 0.03[c]	3.71 ± 0.03[b]	ND	3.15 ± 0.03[b]	1.45 ± 0.03[a]	1.20 ± 0.03[a]	2.00 ± 0.03[a]	ND
20	8.10 ± 0.03[b]	2.17 ± 0.03[a]	ND	2.08 ± 0.03[a]	0.72 ± 0.03[a]	0.89 ± 0.03[a]	1.78 .± 0.03[a]	ND
CTRL	6.01 ± 0.140[b]	2.36 ± 0.42[ab]	1.08 ± 0.02[a]	1.10 ± 0.09[a]	1.01 ± 0.20[a]	0.10 ± 0.01[a]	2.15 ± 0.15[ab]	0.06 ± 0.10[a]

The data presented are expressed as the mean ± standard error (SE). A one-way ANOVA was conducted, and results with $p < 0.05$ indicate significant differences in means among groups. The control group is denoted as such. Values that were not detected or are not applicable are indicated accordingly as ND. Different letters (a, b, c) signify significant differences in means among groups as determined by post-hoc tests, such as Tukey's HSD; CTRL: Unpolluted soil.

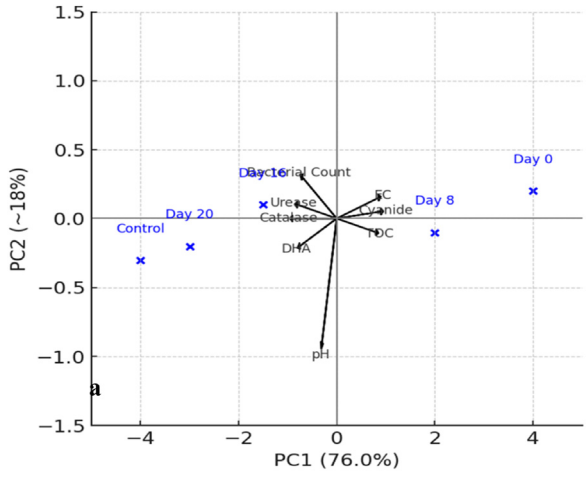


Fig. 3a. PCA Biplot: Soil Properties vs Microbial Activity. This biplot illustrates the relationships among pH, cyanide, microbial activity indices (e.g., catalase, urease, DHA), and treatment days, showing divergence between polluted and treated soils.

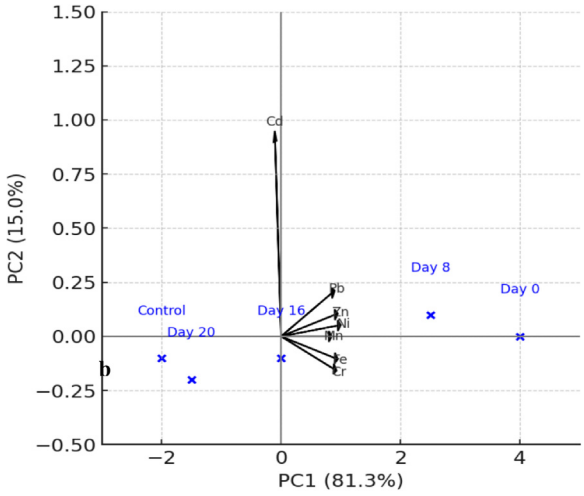


Fig. 3b. PCA Biplot: Heavy Metal Correlations. The biplot illustrates relationships among heavy metals (Cd, Pb, Zn, Ni) and sampling days based on PC1 (81.3 %) and PC2 (15.0 %).

ness of bioremediation in reducing pollution load and re-establishing soil health.

Fig. 4 presents a phylogenetic tree based on 16S rRNA gene sequences of cyanide-degrading bacterial isolates (IBR-001 to IBR-004) and their closely related strains. The tree shows the evolutionary relationships among these isolates, with bootstrap values indicating the confidence of the branching patterns. The accession numbers in parentheses correspond to the isolates' identification codes, and the tree highlights their potential genetic basis for cyanide degradation

The Cryo-EM structure of nitrilase from *Pseudomonas fluorescens* EBC191, resolved at 3.3 Å, reveals key interactions within its binding site, as depicted in Fig. 5. The 3D structure highlights interactions with residues such as Ala150, Arg128, Thr127, Asp148, Ala126, Ser147, and His152, where hydrogen bonds (visualized as green dashed lines) and van der Waals forces contribute to substrate binding. The 2D schematic further illustrates these interactions, detailing hydrogen bond distances that range from 2.86 Å (Arg128) to 3.57 Å (Thr127). These molecular interactions result in a binding energy of 1.4 kcal/mol, indicating moderate substrate affinity. Together, the 2D and 3D analyses provide a comprehensive view of the binding site, offering valuable insights for enhancing the enzyme's catalytic efficiency through structural or mutational modifications.

Panel B: Cyanide dihydratase (*B. pumilus*; PDB 8P4I) 3D model showing substrate binding.

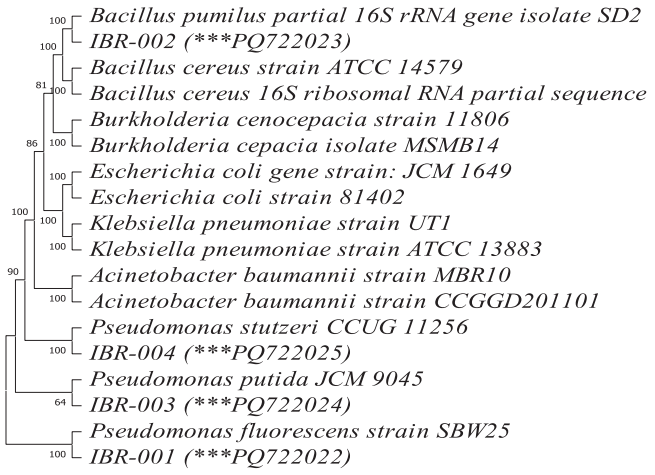


Fig. 4. Phylogenetic Tree Based on 16S rRNA Gene Sequences of Cyanide-Degrading Bacteria.

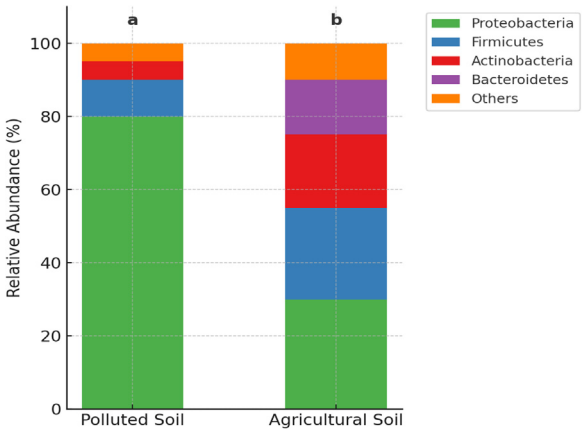


Fig. 6a. Relative abundance of bacterial phyla in CME-polluted soil and Agricultural soil.

a: LigPlot of nitrilase-CN^- interactions (key residues: Thr127, Arg128, Ser147, Asp148, His152).

b: LigPlot of dihydratase active site (Glu60, Lys128, Arg101, Cys175, His235).

Green dashes = *H*-bonds; blue/purple = polar/basic residues. Confirms stable CN^- binding in both enzymes.

The structure of cyanide dihydratase from Bacillus pumilus C1, resolved at 3.83 Å, highlights molecular interactions within its binding site, as shown in the 3D visualization. Key residues involved in the binding include those forming hydrogen bonds and van der Waals interactions with the substrate. The hydrogen bond distances, indicated by green dashed lines, range from approximately 3.06 Å to 3.61 Å, suggesting moderate binding stability. The binding energy of −1.2 kcal/mol indicates weak exergonic interaction, which might necessitate modifications to improve substrate affinity. The 2D schematic illustrates the interaction network within the enzyme's binding pocket. Hydrogen bonds, van der Waals forces, and key residues contributing to binding are shown, with hydrogen bond distances annotated. This provides a comprehensive overview of the enzyme-substrate interaction profile, supporting structural insights into the binding energy of −1.2 kcal/mol. This structure provides a detailed view of the enzyme's active site, which can inform future optimization efforts, such as mutagenesis or computational studies, to enhance catalytic efficiency.

Fig. 6a compares the relative abundance of bacterial phyla in polluted soil versus agricultural soil. In the polluted soil, Proteobacteria dominates, making up over 80 % of the bacterial community, with

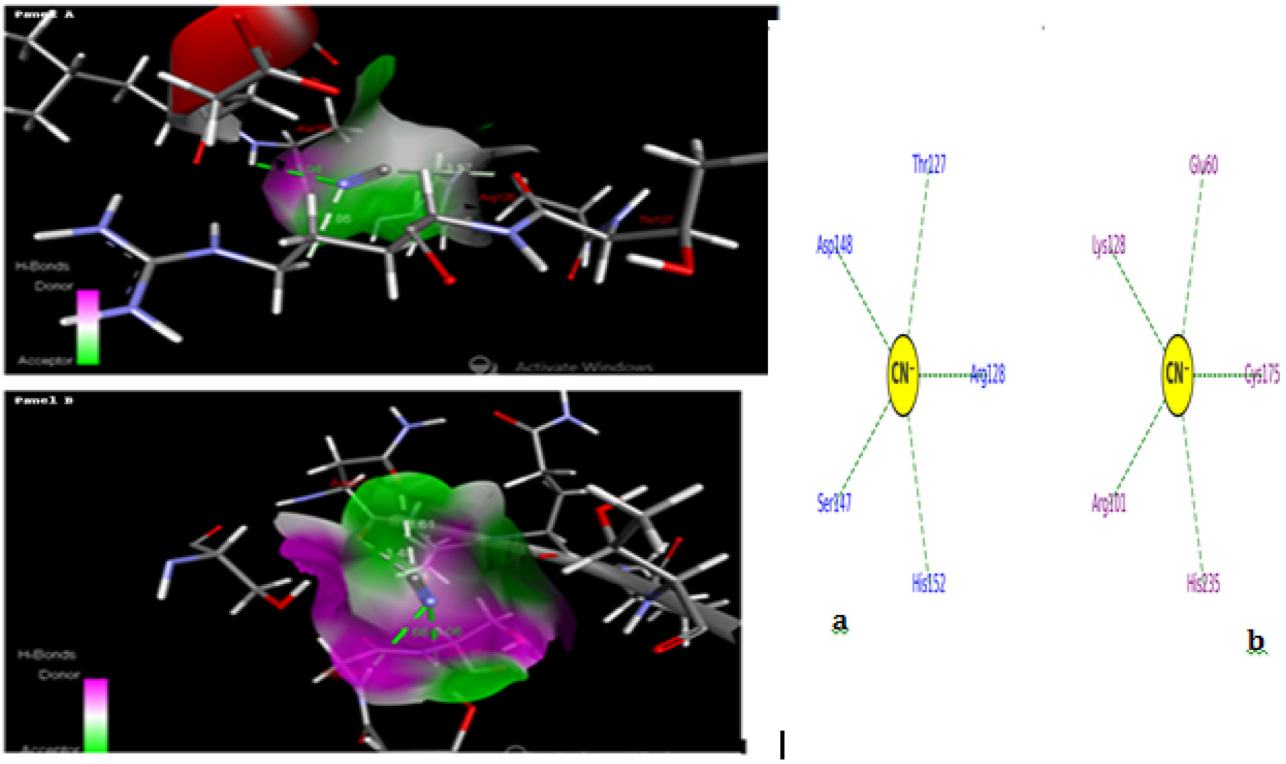


Fig. 5. Structural and LigPlot Representations of Enzyme–Cyanide Interactions.
Panel A: Nitrilase (*P. fluorescens*) 3D structure with CN^- bound in active site (magenta/green = *H*-bond donor/acceptor surfaces).

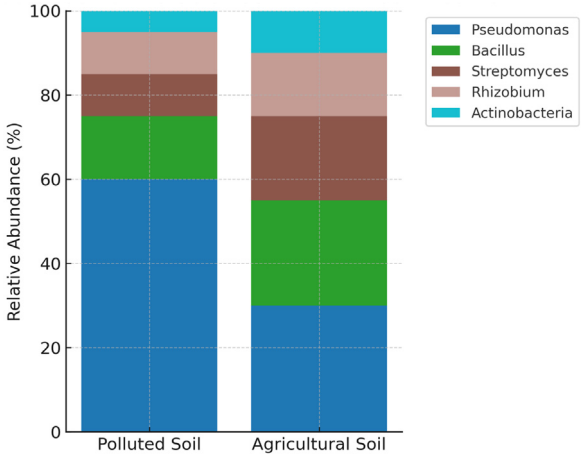


Fig. 6b. Relative abundance of bacterial genera in CME-polluted soil and Agricultural soil.

smaller proportions of *Firmicutes, Actinobacteria*, and *Bacteroidetes.* In contrast, agricultural soil still has a dominant presence of *Proteobacteria,* but its proportion is lower (around 60 %) compared to polluted soil. Agricultural soil supports a more diverse microbial community, with higher proportions of *Firmicutes* and *Bacteroidetes.* This suggests that agricultural soil likely has a more balanced microbial ecosystem, while the polluted soil is largely dominated by *Proteobacteria,* indicating a disruption in microbial diversity due to contamination. Fig. 6b compares the relative abundance of bacterial genera in CME-polluted soil and agricultural soil. In polluted soil, *Pseudomonas* dominates, making up over 60 % of the bacterial community, with smaller proportions of *Bacillus, Streptomyces, Rhizobium,* and *Actinobacteria.* In contrast, agricultural soil shows a more balanced community, with a reduced proportion of *Pseudomonas* and higher representations of *Bacillus, Streptomyces, Rhizobium,* and *Actinobacteria*, indicating greater microbial diversity. The results suggest that agricultural soil supports a more diverse and potentially beneficial microbial community compared to the *Pseudomonas*-dominated polluted soil.

5. Discussion

Cassava is an economically significant crop and a primary source of agro-products for various industries, as well as a staple food for millions worldwide, particularly in tropical and subtropical regions. Its tubers are rich in carbohydrates, making cassava a critical energy source for both human consumption and animal feed. The crop also plays a pivotal role in industries such as starch production, bioethanol manufacturing, and animal feed production, contributing to economic growth and food security in developing countries. However, the byproducts of cassava processing, particularly cassava mill effluents (CME), pose significant environmental challenges.

Effluent discharge from cassava mills often contaminates surrounding soils, altering their physicochemical properties and microbial ecology. Studies have shown that soils impacted by CME exhibit lower pH levels due to acidification caused by organic acids and cyanogenic compounds, leading to degraded soil fertility and productivity [9]. These soils also demonstrate increased electrical conductivity and nutrient imbalances, with elevated total nitrogen and organic carbon levels but reduced phosphorus availability [10]. Moreover, heavy metal contamination from CME further compromises soil health, with higher concentrations of metals such as iron, zinc, and manganese observed in polluted sites [11].

Previous studies extensively highlight the significant alterations in soil physicochemical properties and microbial profiles caused by cassava mill effluent pollution. For instance, soils contaminated with cassava mill effluent exhibit pronounced acidification, with pH values significantly lower than those of unpolluted controls due to the effluent's organic acid content and cyanogenic compounds (Worlanyo and Jiangfeng, 2020). Similarly, the electrical conductivity of polluted soils is elevated, reflecting higher ionic concentrations derived from dissolved salts in the effluent [12]. Furthermore, organic carbon and total nitrogen levels increase significantly in polluted soils, suggesting nutrient enrichment—albeit potentially harmful due to imbalanced nutrient dynamics [13]. In contrast, phosphorus content typically decreases, likely due to precipitation reactions in acidic conditions (Wang *et al.*, 2021).

The effluent's cyanide concentration also poses a severe hazard, with significantly elevated levels in polluted soils compared to controls, originating from cyanogenic glucosides in cassava waste ([14]. Heavy metal enrichment, including iron, zinc, and manganese, is another notable consequence, although some metals, such as lead and chromium, may not show significant variation [15]. Microbial studies consistently report decreased total heterotrophic bacterial counts and cyanide-degrading bacterial populations in polluted soils compared to unpolluted controls, with variations attributable to effluent-induced toxicity and altered soil conditions [16].

The enzymatic activity data provide key insights into the potential of various bacterial isolates for further molecular studies, particularly in the context of cyanide and heavy metal detoxification. Among the bacterial isolates tested, *Pseudomonas fluorescens* stands out due to its remarkable enzymatic activities, specifically for Cyanide Dioxygenase (0.37 U/mg) and Nitrilase (3.22 U/mg). These high activity levels suggest that *P. fluorescens* has significant potential for cyanide detoxification, making it an ideal candidate for further molecular analysis aimed at understanding the biochemical mechanisms involved in cyanide degradation. Cyanide is a highly toxic substance that poses environmental and health risks, especially in industrial areas where cyanide compounds are frequently released into the environment. The high Nitrilase activity of *P. fluorescens* is particularly noteworthy, as nitrilases are known to catalyze the hydrolysis of nitriles to carboxylic acids, a process that could contribute to the detoxification of cyanide and other nitrile-containing pollutants.

In contrast to *P. fluorescens, Bacillus pumilus* demonstrates exceptional activity in another key enzymatic pathway, specifically for Cyanide Dihydratase, where it exhibits an activity of 3.33 U/mg. This value is significantly higher than that of the other bacterial isolates tested, making *B. pumilus* a highly promising candidate for further investigation. Cyanide Dihydratase plays a crucial role in the detoxification of cyanide by converting it into less toxic intermediates. The outstanding activity of *B. pumilus* in this enzyme suggests that it could be particularly effective in remediating environments contaminated with cyanide, making it an excellent subject for further studies on cyanide bioremediation.

Additionally, the analysis of Rhodanese activity reveals some interesting findings. *Pseudomonas stutzeri* exhibits a slightly higher activity (0.35 U/mg) compared to *Pseudomonas fluorescens* (0.30 U/mg) in this enzyme's activity, which is involved in detoxifying sulfur-containing compounds, including cyanide. While the differences in activity are modest, the data suggest that both *P. stutzeri* and *P. fluorescens* could be valuable in bioremediation efforts targeting sulfur compounds, with potential applications in industries that deal with cyanide-based pollutants.

The highest-producing enzymes in this study—Cyanide Dihydratase from *B. pumilus* and Nitrilase from *P. fluorescens*—are therefore the most suitable candidates for molecular docking studies with cyanide ions. These studies could explore the molecular mechanisms of cyanide degradation and provide a deeper understanding of how these enzymes function at the atomic level. The potential to design inhibitors or enhancers of these enzymatic pathways could lead to more efficient bioremediation strategies for cyanide and other toxic substances in contaminated environments.

The bioremediation data presented in this study further highlight the effectiveness of the bacterial isolates in remediating soil polluted with cassava mill effluent over a 20-day period. The results indicate significant improvements in various soil parameters, pointing to the effectiveness of the microbial treatments in enhancing soil health and detoxifying pollutants. Cyanide concentration, a key contaminant of concern, decreases drastically from 310.96 mg/kg on day 0 to 42.98 mg/kg on day 20, a value that approaches the control group's cyanide level of 21.00 mg/kg. This significant reduction in cyanide concentration reflects the active involvement of the microbial community in cyanide degradation, with the bacterial isolates likely contributing through enzymatic processes like those described earlier. The soil pH also increases from 4.8 to 7.4, suggesting that microbial activity is driving the soil towards more neutral conditions, which is beneficial for plant growth and overall soil health.

Other indicators of soil quality, such as cation exchange capacity (CEC), also show substantial improvements during the bioremediation process. The CEC rises from 1.35 cmol/kg to 6.87 cmol/kg, which is indicative of enhanced soil fertility and an improved ability to retain essential nutrients. This is likely due to the metabolic activities of the bacteria, which help in the transformation of organic and inorganic compounds in the soil. Bacterial populations in the soil grow significantly, peaking at 7.02 log cfu/g on day 12 before stabilizing, which indicates that the bacteria are actively colonizing the soil and contributing to the degradation of pollutants. Enzyme activities, such as those of urease, dehydrogenase, and catalase, also show an increase, further confirming the active microbial degradation and metabolic processes that are enhancing soil health. Additionally, total organic carbon (TOC) declines from 11.98 % to 2.88 %, and electrical conductivity (EC) decreases from 237.60 μS/cm to 90 μS/cm, reflecting improved soil quality and reduced salinity, which can otherwise hinder plant growth.

The results provide additional evidence of the effectiveness of the bioremediation process, specifically in relation to heavy metal contamination. Over the 20-day period, there is a progressive reduction in the concentrations of several heavy metals in the soil, including iron (Fe), manganese (Mn^{2+}), copper (Cu^{2+}), cadmium (Cd^{2+}), zinc (Zn^{2+}), chromium (Cr^{6+}), lead (Pb^{2+}), and nickel (Ni^{2+}). Notably, copper is completely removed by day 16, and cadmium becomes undetectable by day 12, demonstrating the rapid and effective action of the bacterial isolates in removing these toxic metals. The concentrations of iron and manganese decrease steadily, while zinc and chromium show significant reductions over the course of the study. The levels of lead and nickel also decrease considerably, indicating that the remediation process is not only effective in removing the most toxic metals but also in reducing the overall burden of heavy metal contamination in the soil. These reductions are markedly better than the control group, which showed minimal natural attenuation, further emphasizing the superior performance of the bacterial treatment.

The observed decline in heavy metal concentrations can be attributed to several microbial-mediated mechanisms of metal removal. One of the primary pathways is biosorption, where metal ions bind to functional groups (e.g., carboxyl, hydroxyl, amino, and phosphate groups) present on the bacterial cell walls (Gadd, 2010; Volesky & Holan, 1995). Bioaccumulation also plays a critical role, involving the active uptake and intracellular sequestration of metals by living bacterial cells (Wuana & Okieimen, 2011). Furthermore, enzymatic biotransformation may occur, particularly in the case of chromium and lead, where specific microbial enzymes reduce highly toxic metal ions (e.g., Cr^{6+} to Cr^{3+}) into less toxic and less mobile forms (Chatterjee et al., 2018). Precipitation and complexation mechanisms contribute to metal immobilization through the formation of insoluble compounds such as metal sulfides or phosphates (Gupta & Diwan, 2017). Additionally, extracellular polymeric substances (EPS) produced by bacteria can effectively trap and immobilize metals, thereby reducing their mobility and bioavailability (Pal & Paul, 2008; Mishra & Malik, 2013). These synergistic mechanisms highlight the multifaceted capabilities of the microbial consortia used in this study and provide a scientific basis for their application in field-scale bioremediation of heavy metal-polluted environments. The use of engineered plant and microbial systems, such as modified tobacco platforms for protein expression, also shows promise for enhancing pollutant removal processes through synthetic biology approaches [17]. This parallels microbial optimization efforts where targeted gene suppression or overexpression improves detoxification outcomes.

The data highlight the strong potential of bacterial isolates such as *Pseudomonas fluorescens* and *Bacillus pumilus* in the bioremediation of both cyanide and heavy metal-contaminated environments. The enzymatic activities observed in these isolates, particularly for Cyanide Dihydratase and Nitrilase, position them as prime candidates for further molecular studies aimed at understanding and enhancing their bioremediation capabilities. The soil remediation data also provide compelling evidence that these bacterial treatments can significantly improve soil quality, reduce toxic pollutants, and promote healthier soil conditions, making them viable candidates for large-scale bioremediation applications.

The Principal Component Analysis (PCA) biplot provides a comprehensive visualization of the relationships between various variables influencing the bioremediation of cassava mill effluent-polluted soil. The first and second principal components (PC1 and PC2) explain a substantial 95.1 % of the variation in the dataset, with PC1 accounting for 76.0 % and PC2 for 19.1 %. This indicates that the majority of the variability in the bioremediation process can be captured by these two components, making PCA a valuable tool for identifying key factors affecting remediation outcomes [18].

Key variables such as cation exchange (CA), dehydrogenase activity (DHA), urease activity (UA), bacterial count, electrical conductivity (EC), and total organic carbon (TOC) are all strongly positively correlated, meaning that as one of these variables increases, the others tend to increase as well. These variables are critical to the success of bioremediation, suggesting that microbial activity and soil health are vital drivers of remediation processes [19]. Dehydrogenase and urease activities, which are indicative of microbial metabolic activity, are directly associated with the soil's ability to detoxify pollutants like cyanide. A higher bacterial count also signifies more active microbial communities that play a significant role in pollutant degradation. Moreover, variables like EC and TOC reflect the overall health and structure of the soil, both of which are crucial for supporting microbial life and enhancing bioremediation processes [20].

On the other hand, cyanide shows a strong negative correlation with these variables, positioning it as a pollutant marker. This negative correlation underscores the toxic nature of cyanide, which inhibits microbial activity and degrades soil health, making it a critical factor to monitor during bioremediation [21]. Cyanide's negative association with soil health parameters highlights its detrimental impact on the bioremediation process, further emphasizing the need to target and degrade this compound for successful remediation.

Soil pH appears distinct from the other variables, being negatively correlated with cyanide but only weakly associated with the other parameters. This suggests that while soil pH plays a role in cyanide detoxification, its effect on overall bioremediation may be less significant compared to the microbial and soil health variables [22]. The proximity of certain samples to microbial activity variables—such as samples 6 and 7—demonstrates effective bioremediation outcomes. These samples show reduced cyanide levels and improved soil quality, reinforcing the notion that microbial activity is a key driver of remediation success.

The PCA biplot also highlights the relationships between heavy metal concentrations in the soil. PC1 and PC2 together explain 96.3 % of the variance in the dataset, with PC1 capturing the majority of the variation (81.3 %). Heavy metals such as zinc (Zn), lead (Pb), manganese (Mn), chromium (Cr), nickel (Ni), and iron (Fe) are grouped closely together, indicating strong positive correlations among these metals. This suggests that these metals behave similarly in the soil environment, possibly due

to shared sources or similar chemical properties [23]. In contrast, cadmium (Cd) is positioned separately on the biplot, reflecting its distinct behavior compared to the other metals. This could be due to differences in its mobility, bioavailability, or interaction with soil components. Samples closer to the cluster of metals (such as samples 2 and 3) are likely characterized by higher concentrations of these correlated metals, while those further from the cluster (like sample 7) may show lower concentrations or different metal profiles. This PCA analysis highlights the variation in heavy metal contamination within the soil and underscores the unique behavior of cadmium, which may require distinct remediation strategies.

The phylogenetic tree based on 16S rRNA gene sequences of cyanide-degrading bacterial isolates (IBR-001 to IBR-004) provides insight into the genetic basis for cyanide degradation. The tree shows the evolutionary relationships among these isolates, with bootstrap values indicating the reliability of the branching patterns. The isolates' close genetic relationships to known cyanide-degrading bacteria suggest a shared evolutionary background that may enhance their ability to break down cyanide. Understanding these genetic relationships can inform future studies aimed at optimizing cyanide degradation through selective breeding or genetic modifications [24].

Finally, the Cryo-EM structure of nitrilase from *Pseudomonas fluorescens* EBC191, resolved at 3.3 Å, offers detailed insights into the enzyme's substrate-binding site. The 3D structure reveals key interactions with residues such as Ala150, Arg128, Thr127, Asp148, Ala126, Ser147, and His152, which contribute to substrate binding through hydrogen bonds and van der Waals forces. The binding energy of 1.4 kcal/mol indicates a moderate affinity for the substrate, which could be further enhanced through structural or mutational modifications [25]. This molecular-level understanding of nitrilase activity provides valuable information for improving the enzyme's catalytic efficiency, potentially enhancing its effectiveness in cyanide degradation during bioremediation efforts.

Notably, these structural features are consistent with the earlier observed catabolic potential of *P. fluorescens*, which demonstrated the highest nitrilase activity (3.22 U/mg) among all tested bacterial isolates. This high activity aligns with the structural evidence of a well-configured active site capable of accommodating and stabilizing nitrile substrates. The ability of *P. fluorescens* to degrade cyanide efficiently can thus be attributed not only to its enzymatic profile but also to the favorable orientation and interaction of catalytic residues within its nitrilase binding pocket. Such dual evidence of function and form underscores the potential of this isolate in the development of targeted bioremediation strategies.

Similarly, the structure of cyanide dihydratase from *Bacillus pumilus* C1, resolved at a high resolution of 3.83 Å, provides detailed insights into the enzyme's molecular interactions within its active site. This structure reveals key residues that play an important role in the enzyme's catalytic function, especially in its interaction with cyanide. The enzyme's binding site is characterized by hydrogen bonds and van der Waals interactions between the enzyme and substrate. The hydrogen bond distances, indicated by green dashed lines in the 3D model, range from approximately 3.06 Å to 3.61 Å, suggesting a moderate level of binding stability. These distances are indicative of the enzyme holding the substrate tightly enough to facilitate the reaction, but not with exceptional strength, allowing for substrate release after catalysis. Such moderate binding is typical for enzymes that need to interact with toxic compounds like cyanide, where too strong an affinity could hinder effective detoxification processes.

These findings also align with the prior functional data, where *B. pumilus* exhibited the highest cyanide dihydratase activity (3.33 U/mg), surpassing other isolates. The structural architecture of the active site thus confirms the biochemical potency of this enzyme, explaining its superior performance in cyanide breakdown. The moderate binding energy observed complements the biological need for efficient catalysis and rapid substrate turnover. Together, the structural and enzymatic data suggest that *B. pumilus* is particularly well-adapted for environments contaminated with high cyanide concentrations, offering a strong candidate for application in microbial detoxification systems.

The convergence of enzymatic activity and structural evidence reinforces the potential of both P. fluorescens and B. pumilus as effective agents in cyanide bioremediation. Their characterized enzyme-substrate interactions not only validate their biochemical profiles but also provide molecular templates for future optimization through protein engineering. The binding energy of −1.2 kcal/mol further reflects the relatively weak exergonic interaction between the enzyme and the substrate. These insights resonate with findings in plant genomics where CRISPR/Cas editing has been applied to improve stress resistance in crops such as tomato, suggesting future potential for microbial gene editing in improving pollutant resilience [26].

This energy suggests that while the binding is energetically favorable, it is not highly intense, indicating room for improvement in substrate affinity. This weak binding energy could limit the enzyme's efficiency, particularly in environments with high cyanide concentrations, where stronger binding might be needed to effectively detoxify the substrate. Future optimization strategies, such as mutagenesis or computational design, could focus on enhancing the binding strength by altering key residues within the enzyme's active site to improve its catalytic efficiency and substrate affinity (Chowdhury & Maranas, 2019).

Furthermore, the 2D schematic of the enzyme-substrate interaction provides a simplified representation of the active site, showing how hydrogen bonds and van der Waals interactions work together to stabilize the substrate within the binding pocket. The schematic also annotates the hydrogen bond distances, providing a clearer view of the molecular interaction network. These insights are essential for understanding how small changes in the enzyme's structure can have a significant impact on its function, and they open pathways for future experimental designs aimed at improving enzyme performance. Interestingly, plant studies have shown how strigolactones and phytohormones regulate fruit ripening through altered biosynthetic pathways [27], an analogy that may guide future research into how microbial metabolic signaling can be tuned to enhance cyanide degradation.

Advances in metagenomics and bioinformatics are transforming soil bioremediation by enabling precise identification of pollutant-degrading microbes, including uncultivable strains. These tools reveal key degraders like Pseudomonas and Bacillus spp., allowing tailored microbial consortia for site-specific cleanup of toxins like cyanide and phenols in cassava mill wastes. Recent studies have explored the epigenetic regulation of plant responses to heavy metal stress [28], suggesting a possible frontier in microbial epigenetic adaptation for enhanced pollutant remediation under variable soil conditions.

Iqbal et al. [29] highlight how omics-guided approaches enhance microbial therapies by matching strains to contamination profiles. Integrating genetic engineering and systems biology further optimizes degradation while preserving soil ecosystems. This precision bioremediation framework offers scalable, sustainable solutions for environmental restoration.

Moving on to the comparison between two soil types, the distribution of various categories in cassava mill effluent-polluted soil and agricultural soil reveals notable differences. In the polluted soil, a single dominant category occupies the majority of the sscomposition, suggesting that the effluent has introduced a predominant component, likely related to organic compounds or contaminants that significantly alter the natural soil balance. This overrepresentation of a single component indicates a loss of diversity in the polluted soil, which is characteristic of environments affected by industrial effluents. The smaller remaining segments imply a reduction in the diversity of soil constituents, which could hinder microbial diversity, nutrient cycling, and overall soil health [30]. Comparable shifts in microbial diversity and dominant genera have been observed in arsenic-contaminated environments, where phytobial interactions significantly improved metal tolerance and ecosystem recovery [31].

In contrast, the agricultural soil shows a more balanced distribution of categories. While a dominant category is still present, it is less pronounced compared to the polluted soil and the proportions of other components are more varied. This reflects a more natural and diverse composition, which is essential for maintaining soil fertility and supporting microbial ecosystems that are critical for nutrient cycling and plant growth [32]. The comparison highlights the detrimental effects of cassava mill effluent pollution on soil biodiversity and composition, which can lead to a decrease in agricultural productivity and environmental sustainability.

6. Conclusion

Cassava mill effluent (CME) pollution significantly impairs soil quality by lowering pH, increasing electrical conductivity, and introducing high levels of cyanide and heavy metals. These changes disrupt microbial communities and suppress enzymatic activity essential for soil health. This study demonstrates that bioaugmentation with cyanide-degrading bacteria, particularly Pseudomonas fluorescens and Bacillus pumilus, effectively mitigates these effects. Within 20 days, soil pH normalized, cyanide concentrations dropped by over 80 %, and key heavy metals (Cd, Cu) were reduced to undetectable levels. Enzyme activity and microbial abundance also improved, indicating biological restoration of the soil. Molecular docking confirmed the catalytic roles of the selected strains, while principal component analysis linked microbial activity with pollutant reduction. These findings support the use of targeted microbial consortia as a sustainable bioremediation strategy for CME-contaminated soils. However, field-based trials are necessary to validate long-term effectiveness and scalability.

Declaration of generative AI and AI-assisted technologies in the writing process

During the preparation of this work the author(s) used CHATGPT in order to improve the grammar. After using this chatgpt, the author(s) reviewed and edited the content as needed and take(s) full responsibility for the content of the publication.

Funding

This research was supported by the Tertiary Education Trust Fund (TETFund) under the Institutional-Based Research (IBR) grant awarded to Kwara State University, Malete. under the Grant Reference Number (KWASUIBR/CRIT/270921/VOL1/TETF2020/0002).The authors sincerely appreciate TETFund for their financial support in conducting this study.

Accession numbers

The 16S rRNA gene sequences of all isolates have been deposited in the GenBank database of NCBI under the accession numbers: *Pseudomonas fluorescens* (IBR-001, PQ722022), *Pseudomonas putida* (IBR-003, PQ722024), *Pseudomonas stutzeri* (IBR-004, PQ722025), and *Bacillus pumilus* (IBR-002, PQ722023).

Data availability declarations in your manuscript

The datasets supporting the findings of this study are fully presented within the manuscript

Declaration of competing interest

The authors declare that they have no known competing financial interests or personal relationships that could have appeared to influence the work reported in this study.

CRediT authorship contribution statement

A.T. Ajao: Writing – review & editing, Writing – original draft, Methodology, Funding acquisition, Data curation, Conceptualization. **S. Awe:** Validation, Supervision, Project administration. **W.T. Aborisade:** Writing – review & editing, Validation, Methodology, Investigation. **F.A. Jimoh:** Writing – review & editing, Project administration, Investigation, Conceptualization. **F.J. Ajao:** Writing – review & editing, Software, Validation, Data curation, Visualization.

Supplementary materials

Supplementary material associated with this article can be found, in the online version, at doi:10.1016/j.nexres.2025.100439.

References

[1] S.C. Izah, G. Richard, T.C. Odubo, A.O. Aigberua, Biodegradation potentials of cassava wastewater by indigenous microorganisms, in: Springer Ebooks, 2022, pp. 443–470, doi:10.1007/978-3-030-99858-5_19.
[2] A.C. Maciel, R. da Silva Pena, L.D. do Nascimento, T.A. de Oliveira, G.C.A. Chagas-Junior, A.S. Lopes, Health exposure risks and bioremediation of cyanide in cassava processing effluents: an overview, J. Water. Proc. Eng. 55 (2023) 104079.
[3] T. Hussain, R. Dhanker, Science of microorganisms for the restoration of polluted sites for safe and helathy environment, in: Elsevier Ebooks, 2021, pp. 127–150, doi:10.1016/b978-0-12-822503-5.00026-6.
[4] N. Kuppan, M. Padman, M. Mahadeva, S. Srinivasan, R. Devarajan, A comprehensive review of sustainable bioremediation techniques: eco friendly solutions for waste and pollution management, Waste Management. Bulletin. 2 (3) (2024) 154–171, doi:10.1016/j.wmb.2024.07.005.
[5] Fasesan, D.E. (2023). Physiological characteristics, amylase properties and metagenomic analyses of bacterial and fungal communities from Ikogosi Warm Springs (Doctoral Dissertation).
[6] M.A. Gumaa, A.B. Idris, N.E. Bilal, M.A. Hassan, First insights into molecular basis identification of 16 s ribosomal RNA gene of Staphylococcus aureus isolated from Sudan, BMC. Res. Notes. 14 (1) (2021) 240.
[7] P. Kharnaior, J.P. Tamang, Probiotic properties of lactic acid bacteria isolated from the spontaneously fermented soybean foods of the eastern himalayas, Fermentation 9 (5) (2023) 461.
[8] G. Adam, H. Duncan, Development of a sensitive and rapid method for the measurement of total microbial activity using fluorescein diacetate (FDA) in a range of soils, Soil Biol. Biochem. 33 (7–8) (2001) 943–951.
[9] L.P. Adjei, E.K. Arthur, E. Gikunoo, G. Foli, J.A. Quaye-Ballard, F.O. Agyemang, D.S. Baah, Cyanide contamination assessment via target survey and physicochemical and bacteriological characterization: a case study of Akrofrom-Techiman cassava processing area in Ghana, Environ. Monit. Assess. 195 (4) (2023) 482.
[10] R. Chowdhury, C.D. Maranas, From directed evolution to computational enzyme engineering—A review, AIChE J. 66 (3) (2020) e16847.
[11] S. Huang, N. Yamaji, J. Feng, Metal transport systems in plants, Annu Rev. Plant Biol. 75 (1) (2024) 1–25, doi:10.1146/annurev-arplant-062923-021424.
[12] A. Quddoos, K. Muhmood, I. Naz, R.W. Aslam, S.Y. Usman, Geospatial insights into groundwater contamination from urban and industrial effluents in Faisalabad, Discover Water 4 (1) (2024) 50.
[13] S.S. Dhaliwal, S.K. Dubey, D. Kumar, A.S. Toor, S.S. Walia, M.K. Randhawa, G. Kaur, S.K. Brar, P.A. Khambalkar, Y.S. Shivey, Enhanced organic carbon triggers transformations of macronutrients, micronutrients, and secondary plant nutrients and their dynamics in the soil under different cropping systems-A review, J. Soil. Sci. Plant Nutr. 24 (3) (2024) 5272–5292, doi:10.1007/s42729-024-01907-6.
[14] C.C. Nnaji, C.C. Akanno, Assessment of environmental degradation due to processing of cassava into Garri flakes using pollution indices, Environ. Proc. 9 (3) (2022) 46.
[15] N. Munir, M. Jahangeer, A. Bouyahya, N. El Omari, R. Ghchime, A. Balahbib, M.A. Shariati, Heavy metal contamination of natural foods is a serious health issue: a review, Sustainability. 14 (1) (2021) 161.
[16] M.Y.A. Shukor, Bacterial reduction of molybdenum as a tool for its bioremediation, CRC Press eBooks (2024) 238–277, doi:10.1201/9781003423393-12.
[17] R. Han, A. Xu, Y. Wang, J. Cao, M. Naeem, W. Zhao, L. Zhao, Creating a novel engineered tobacco chassis with downregulated expression of β-1, 2-xylosyltransferase, J. Plant Biochem. Biotechnol. (2024) 1–9.
[18] M. Freedman, K.G. Mumford, A. Danko, D. Hart, S.D. Richardson, Demonstration of a principal component analysis trajectory method to assess bioremediation progress at a TCE-impacted site, Groundwater Monitoring Remediat. 43 (2) (2023) 90–97, doi:10.1111/gwmr.12572.
[19] C. Pan, H. Yang, W. Gao, Z. Wei, C. Song, J. Mi, Optimization of organic solid waste composting process through iron-related additives: a systematic review, J. Environ. Manage 351 (2024) 119952.
[20] J. Ou, X. Luo, J. Liu, L. Huang, L. Zhou, Y. Yuan, Predicting microbial extracellular electron transfer activity in paddy soils with soil physicochemical properties using machine learning, Sci. China Technol. Sci. 67 (1) (2023) 259–270, doi:10.1007/s11431-023-2537-y.

[21] Y. Wang, Z. Chen, D. Hu, L. Jiang, S. Cui, S. Zhuang, Z. Liang, Optimization of ethylene thiourea, cyanide, and heavy metals removal and gas production enhancement in organosulfur pesticide wastewater using ferromagnetic biochar in anaerobic membrane bioreactor, Chem. Eng. J. 496 (2024) 153785.
[22] A. Cosmos, B. Erdenekhuyag, G. Yao, H. Li, J. Zhao, W. Laijun, X. Lyu, Principles and methods of bio detoxification of cyanide contaminants, J. Mater. Cycles. Waste Manage 22 (4) (2020) 939–954, doi:10.1007/s10163-020-01013-6.
[23] Q. Li, Y. Wang, Y. Li, L. Li, M. Tang, W. Hu, S. Ai, Speciation of heavy metals in soils and their immobilization at micro-scale interfaces among diverse soil components, Sci. Total Environ. 825 (2022) 153862.
[24] Juma, B.S. (2022). *Generation of Cassava with reduced levels of cyanogens through CRISPR/Cas9 targeted mutagenesis of the cytochrome P450 (CYP79D1) gene* (Doctoral dissertation, JKUAT-IBR).
[25] S. Qiu, C.L. Ju, T. Wang, J. Chen, Y.T. Cui, L.Q. Wang, J. Huang, Evolving ω-amine transaminase At ATA guided by substrate-enzyme binding free energy for enhancing activity and stability against non-natural substrates, Appl. Environ. Microbiol. 90 (7) (2024) e00543-24.
[26] M. Naeem, W. Zaman, S. Saqib, A. Shahzad, S. ur Rahman, N. Ahmad, CRISPR/Cas-mediated genome editing for efficient tomato breeding: past achievements and future directions, South Afric. J. Botany 172 (2024) 277–288.
[27] M. Naeem, R. Han, A. Xu, X. Shan, L. Zhao, Strigolactone (GR24) regulates fruit ripening in yft3 tomatoes by altering ABA biosynthesis, Plant Sci. 356 (2025) 112484.
[28] B. Iqbal, N. Ahmad, G. Li, A. Jalal, A.R. Khan, X. Zheng, D. Du, Unlocking plant resilience: advanced epigenetic strategies against heavy metal and metalloid stress, Plant Sci. (2024) 112265.
[29] B. Iqbal, G. Li, K.F. Alabbosh, H. Hussain, I. Khan, M. Tariq, Q. Javed, M. Naeem, N. Ahmad, Advancing environmental sustainability through microbial reprogramming in growth improvement, stress alleviation, and phytoremediation, Plant Stress 10 (2023) 100283, doi:10.1016/j.stress.2023.100283.
[30] P.B. George, D.B. Fidler, J.D. Van Nostrand, J.A. Atkinson, S.J. Mooney, S. Creer, D.L. Jones, Shifts in soil structure, biological, and functional diversity under long-term carbon deprivation, Front. Microbiol. 12 (2021) 735022.
[31] S.U. Rahman, X. Liu, M. Khalid, A. Rehman, J. Cao, S.I. Kayani, M. Naeem, N. Ahmad, A.A. Khan, M.A. Manzoor, C. Zhao, H. Tan, X. Li, Y. Bian, J. Xu, N. Hui, Beyond contamination: enhancing plant tolerance to arsenic through phytobial remediation, South Africa. J. Botany 164 (2024) 250–265, doi:10.1016/j.sajb.2023.12.005.
[32] S. Prasad, L.C. Malav, J. Choudhary, S. Kannojiya, M. Kundu, S. Kumar, A.N. Yadav, Soil microbiomes for healthy nutrient recycling, in: Environmental and Microbial Biotechnology, 2020, pp. 1–21, doi:10.1007/978-981-15-6949-4_1.